



CrossMark
 click for updates

Cite this: *RSC Adv.*, 2014, 4, 61691

Excellent gas sensing and optical properties of single-crystalline cadmium sulfide nanowires†

Linghui Zhu,^a Caihui Feng,^c Feng Li,^b Dezhong Zhang,^b Chao Li,^a Ying Wang,^a Ying Lin,^b Shengping Ruan^{*a} and Zhanguo Chen^{*b}

The chemical and optical properties of 1D single-crystalline cadmium sulfide (CdS) nanowires (NWs) synthesized by a solvothermal method were discussed systematically. The CdS NW was characterized using different analytical techniques. In our work, CdS was employed as the active nanomaterial to detect ethanol gas for the first time and showed good gas sensing performance. Especially, the fast response (0.4 s) and recovery speed (0.2 s) to 100 ppm ethanol were much faster than the reported values. The visible-light detector based on CdS NWs demonstrated ultrafast decay speed (3.77 ms), which was the fastest in the reported photodetectors (PDs) based on randomly oriented CdS NW networks. This research indicates that the CdS NW is an excellent nanomaterial for high performance gas sensors and PDs.

Received 23rd September 2014
 Accepted 5th November 2014

DOI: 10.1039/c4ra11010b

www.rsc.org/advances

Introduction

With large surface-to-volume ratios and Debye length comparable to their small sizes, one-dimensional inorganic nanostructures have stimulated an increasing interest over the past two decades due to their specific functional properties. Up to now, nanoscale devices based on metal oxide nanostructures, such as ZnO,¹ SnO₂,² Co₃O₄,³ TiO₂,⁴ In₂O₃,⁵ have been widely reported. However, metal chalcogenides which have the advantages of low cost, chemical stability, easy fabrication and extraordinary optoelectronic properties have received relatively little attention.⁶ As one of the most important II–VI metal chalcogenide semiconductors, CdS has the closest fundamental physical properties with ZnO, one of the few dominant materials in nanotechnology along with Si NWs and carbon nanotubes, including crystal structures, lattice constants and so on.⁷ With a direct band gap (~2.4 eV, at room temperature), relatively low work function (~4.2 eV), large refraction index, excellent thermal and chemical stability, CdS is probably a very promising material for visible-light detectors, sensors, waveguide photodetectors, lasers, field-effect transistors, solar cells and photocatalysis.^{8–11}

Sensing of volatile organic compounds (VOC) is very important for the safety of human life and industrial fields, and

intensive efforts have been made in developing VOC gas sensors based on 1D nanostructured materials in recent years.¹² Though CdS NWs may be advanced functional materials in applications for the detection of chemical vapors, there are very few studies on CdS gas sensors reported in the past years. In 1976, a Pd–CdS Schottky diode was manufactured to detect hydrogen by Martin C. Steele *et al.*¹³ In 1995, V. Smytyna *et al.* produced CdS film by an electrohydrodynamic spray method and studied its oxygen sensing properties.¹⁴ In 2012, B. T. Raut *et al.* fabricated a CdS film sensor to detect H₂S.¹⁵ Apart from these reports above, little has been written about the CdS gas sensors.

As an important application of semiconductor materials, PDs or optical switches are critical for applications in imaging techniques and light-wave communications, as well as future memory storage and optoelectronic circuits.⁷ Due to the direct band gap and high sensitivity, CdS is the most promising material for detecting visible radiation and has recently come to the forefront.^{9,16} In the past, relatively slow response speeds of CdS bulk single crystals and films (>tens of milliseconds) have kept CdS far from the practical demands.¹⁷ Compared with CdS bulk phases or films, 1D CdS NWs have potential charge transport benefits because of the ability to conduct charges efficiently along the length of the wire and often show better photoelectrical performance.¹⁸ Therefore, some 1D CdS nanostructures were used in PD and showed good photoelectrical properties. For example, Lee *et al.* obtained CdS nanoribbons by a chemical vapor deposition (CVD) method and latterly fabricated individual CdS nanoribbon-based visible-light PDs with high photosensitivity and high photoresponse speed in 2006.¹⁹ Liang Li *et al.* constructed individual CdS nanobelt (NB) photoconductive devices with fast speed and high quantum efficiency in 2010. The single-crystalline CdS NBs were

^aState Key Laboratory on Integrated Optoelectronics, Jilin University, Changchun 130012, P. R. China. E-mail: ruansp@jlu.edu.cn

^bCollege of Electronic Science and Engineering, Jilin University, Changchun 130012, P. R. China. E-mail: czg@jlu.edu.cn

^cCollege of Instrumentation and Electrical Engineering, Jilin University, Changchun 130012, P. R. China

† Electronic supplementary information (ESI) available. See DOI: 10.1039/c4ra11010b

synthesized by an improved vapor–liquid–solid (VLS) process.⁹ To date, several kinds of synthetic techniques have been used to prepare 1D CdS nanomaterials which were used in visible-light detection, such as thermal evaporation,^{17,20,21} CVD,¹⁹ VLS,⁹ physical vapor deposition (PVD)⁹ and so on. But up to now, PDs based on randomly oriented NW networks always had slow response and discovery speed to illumination compared with those based on a single NW. Therefore, it remains a challenge to develop a convenient and low-cost method to produce CdS NW PDs with fast speed.

In this experiment, gas sensing and optical properties of single-crystalline CdS NWs prepared by a solvothermal method were studied. The CdS NWs-based gas sensor shows high sensitivity, ultra-fast response (0.4 s) and recovery time (0.2 s), and high selectivity when used to detect ethanol. For the visible-light detector based on CdS NWs, the fabrication process of devices affords the advantages of high efficiency, low-cost and easy mass production. The photo-to-dark conductance ratio of the CdS detector was more than 2 orders of magnitude under 460 nm light irradiation at 4 V bias. The obtained device shows ultra-fast response (750 μ s) upon illumination, which is much quicker than the vast majority of reported 1D CdS devices. The decay speed (3.77 ms) is the fastest in the reported PDs based on randomly oriented CdS NW networks.

Experimental section

Preparation and characterization of CdS NWs

All of the reactants were analytical pure and used without further purification. Uniform CdS NWs were prepared through a simple solvothermal method. In a typical procedure, 1.9 g of cadmium nitrate and 1.4 g of thiourea were added into a Teflon stainless steel autoclave of 50 mL capacity which had been filled with ethylenediamine to 60% of the total volume. After that, the autoclave was maintained at 180 °C for 48 h and then air-cooled to room temperature. Lastly, the solid precipitate was filtered and washed several times with absolute ethanol and distilled water in order to remove residual impurities. The yellow product was dried at 70 °C in air.

The crystal structures of the products were determined by the X-ray diffraction (XRD) method based on a Shimadzu XRD-6000 diffractometer at room temperature. The morphology and the microstructure of the products were analyzed by a field-emission scanning electron microscope (SEM, XL 30 ESEM FEG). A Tecnai G²20S-Twin transmission electron microscope (TEM) was used to observe the morphology of the sample and conduct the energy dispersive X-ray (EDX) analysis. Photoluminescence (PL) measurements were carried out with a He–Cd laser (325 nm, 18 mW). Time-resolved PL studies were performed with the time-correlated single-photon counting (TCSPC) system under right-angle sample geometry. A 405 nm picosecond diode laser (Edinburgh Instruments EPL375, repetition rate 2 MHz) was used to excite the samples. The fluorescence was collected by a photomultiplier tube connected to a TCSPC board. All measurements were performed at room temperature.

Gas sensor fabrication and measurement

To produce the gas sensor, some CdS NWs were mixed with a suitable amount of water after sonication to form a yellow paste. The paste was coated onto a ceramic tube with a pair of Au electrodes attached for resistance measurements. Fig. S1 in the ESI† shows the schematic structure of the CdS NWs gas sensor. After being welded on the pedestal, the gas sensors were aged for 72 h at the work temperature of 120 °C.

The gas sensing properties of the gas sensor were measured by a CGS-8 (Chemical gas sensor-8) intelligent gas sensing analysis system (Beijing Elite Tech Co., Ltd., China). In the gas sensing experiments, the low concentration ethanol gas is prepared by two steps, which is explained in the ESI.† The sensitivity value (S) of the sensor was defined as $S = R_a/R_g$, where R_a is the device resistance in air and R_g is its resistance in the presence of a test gas. The response speed was measured as follows: firstly, the sensor was put into the test bottle with a certain concentration of target gas; secondly, the sensor was taken out to recover in air when the sensitivity reached a constant value. The time taken to achieve 90% of the total sensitivity change was defined as the response time τ_{res} in the case of response (target gas adsorption) or the recovery time τ_{rec} in the case of recovery (target gas desorption).

Visible-light detector fabrication and measurement

The preparation process of the PD is illustrated in Fig. S2 in the ESI.† Firstly, the planar-interdigitated Au electrodes were deposited on the quartz substrate by a magnetron sputtering method after a standard photolithography process. Both the finger width and the separation distance between the electrodes were 30 μ m, and the total active area A was 0.886 mm². Secondly, some CdS NWs were dispersed in a suitable amount of water to form a yellow suspending liquid through sonication. Finally, a few drops of the resulting suspensions were dropped onto the Au electrodes and a CdS NWs-based PD was obtained after the water evaporated. The surface of the substrate is very smooth and water evaporates easily, so the contact between CdS NWs and Au electrodes is good.

The current–voltage (I – V) characteristics and the responsivity of the PD were measured by the Keithley 2601 Source Meter together with a power meter. The monochromatic light was obtained using a 30 W deuterium lamp and a monochromator. The responsivity is calculated by: $R = I_{ph}/AE$. Here, the R , I_{ph} and E are the responsivity, the photon induced current and the irradiance of the light, respectively.

Results and discussion

Composition and morphology of CdS NWs

Fig. 1a and b show the typical SEM image and the magnified SEM image of the CdS NWs with clean and smooth surfaces. The diameters and lengths of NWs are in the range of 30–110 nm and several micrometers, respectively, while each NW is uniform in width and thickness along its length direction. XRD analysis was performed to investigate the crystalline phase of the CdS NWs product and its crystallographic orientation. It is

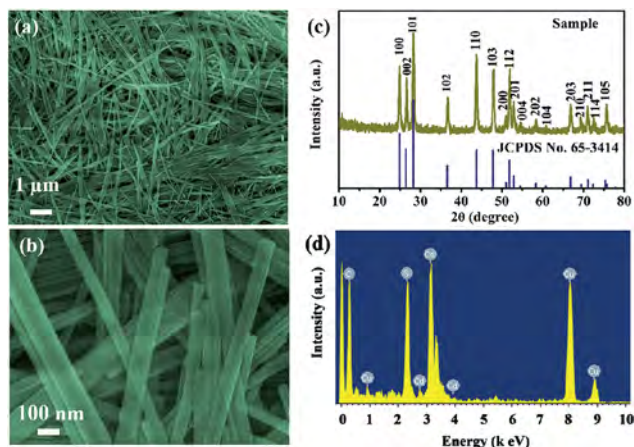


Fig. 1 (a) SEM image and (b) magnified SEM image of the as-synthesized CdS NWs product. (c) XRD pattern of CdS NWs. (d) EDS result of CdS NWs.

clearly seen in Fig. 1c that the diffraction peaks of the product are consistent with the peaks of the hexagonal wurtzite CdS in the JCPDS Card (no. 65-3414), with lattice constants of $a = 4.132 \text{ \AA}$ and $c = 6.734 \text{ \AA}$.²² This indicates that the space group of hexagonal CdS in the pure wurtzite form belongs to $P63mc$. No other crystalline impurities are detected. The EDX result in Fig. 1d was acquired from one area of the as-grown CdS NWs. In addition to C and Cu peaks from a TEM Cu grid, only Cd and S peaks were recorded in the spectrum, showing that the CdS NWs were chemically pure.

Fig. 2a displays the TEM image of CdS NWs. The detailed microstructure of the sample (spot A) was further characterized by the TEM image at high magnification in Fig. 2b. It is noted that the measured interplanar distance (0.67 nm) for the NW lattice corresponds to the (001) lattice spacing of the hexagonal CdS crystal, which has a direction parallel to the long axis of the NWs.⁶ The corresponding selected-area electron diffraction (SAED) pattern (inset) further indicates that the CdS NWs are hexagonal single-crystalline.¹⁹

Gas sensor performance and sensing mechanism

The gas sensing properties of the as-prepared CdS NWs for the detection of ethanol were investigated. In order to determine the optimum operating temperature, the sensitivity of the CdS

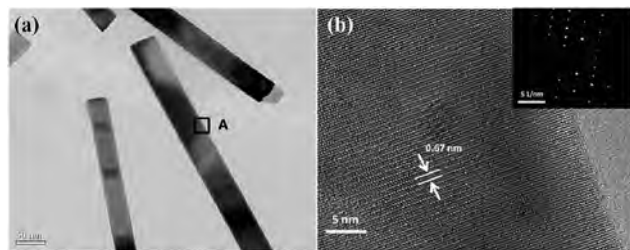


Fig. 2 (a) TEM image of the as-synthesized CdS NWs. (b) HRTEM image of a CdS NW, the corresponding SAED pattern is shown in the inset.

NW-based gas sensors to 100 ppm ethanol gas in air were tested as a function of operating temperature (Fig. S3†). The device exhibits the highest sensitivity value towards ethanol of about 14.9 at 206 °C, which was determined to be the optimum operating temperature and all other gas sensing tests of the as-prepared CdS NWs were conducted at this temperature.

Fig. 3a shows the sensitivity of the sensor as a function of ethanol gas concentration at 206 °C. In the inset, it can be found that the sensitivity increases linearly with the ethanol concentration from 2 to 100 ppm, which makes such devices very practical. Fig. 3b shows the response–recovery curves of the gas sensor towards 20, 50, 100 and 200 ppm ethanol, respectively. The sensitivity values of the sensor underwent a drastic increase when exposed to ethanol and then dropped to its initial values after the sensor was exposed to air. The representative dynamic gas response of the gas sensor to ethanol is shown in Fig. 3c. For 100 ppm ethanol, the response time τ_{res} and recovery time τ_{rec} of the gas sensor based on the CdS NWs are found to be as short as 0.4 s and 0.2 s, respectively, which were the fastest values reported to our best knowledge (Table 1). The selectivity of sensors is very important for their practical applications. It ensures that the sensors can exactly detect the targeted molecules. Thus the sensitivities of the single-crystalline CdS NW-based gas sensor to 100 ppm of various gases, such as ethanol ($\text{CH}_3\text{CH}_2\text{OH}$), methanol (CH_3OH), acetone ($\text{C}_3\text{H}_6\text{O}$), formaldehyde (HCHO), hydrogen sulfide (H_2S), ammonia (NH_3), benzene (C_6H_6) and carbon monoxide (CO) were measured under the same conditions. As shown in Fig. 3d, the sensor exhibits an obvious response for ethanol and lesser effects for other volatile gases, demonstrating that our sensor exhibits high sensing selectivity for ethanol. The above results reveal that the single-

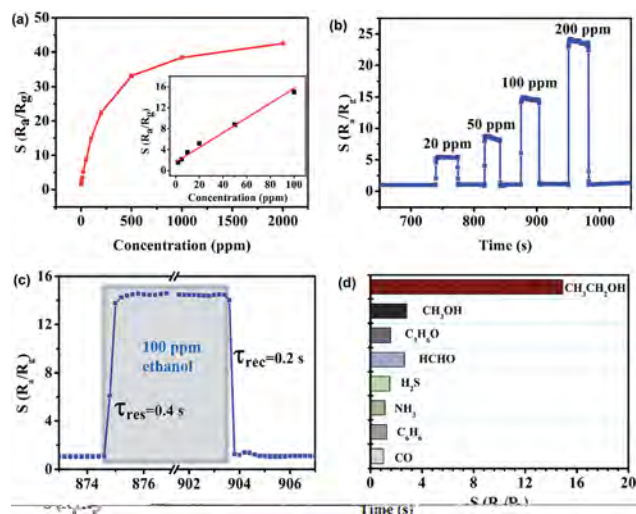


Fig. 3 (a) Sensitivity of the gas sensors at an operating temperature of 206 °C vs. ethanol concentration. The inset shows a linear dependence of the sensitivity on the ethanol concentration in the range 2–100 ppm; (b) response–recovery curves of the gas sensor towards 20, 50, 100 and 200 ppm ethanol, respectively; (c) dynamic gas response of the gas sensor to ethanol at 100 ppm; $\tau_{\text{res}} = 0.4 \text{ s}$ and $\tau_{\text{rec}} = 0.2 \text{ s}$; (d) sensing sensitivity of the gas sensors to different gases with a concentration of 100 ppm at an operating temperature of 206 °C.

Table 1 Comparison of the reported ethanol gas sensors

Material	Work temperature	Response time	Recovery time	Ethanol concentration	Response (R_a/R_g)	Reference
CdIn ₂ O ₄ nanoparticle	260 °C	6 s	30 s	1000 ppm	150	37
CdO film	400 °C	19 s	103 s	1000 ppm	1.28	38
Flower-like α -Fe ₂ O ₃ nanostructure	280 °C	1 s	0.5 s	100 ppm	37.9	39
Flower-like SnO ₂ nanostructure	240 °C	2 s	15 s	100 ppm	42.6	40
Pt@SnO ₂ nanorods	300 °C	2 s	20 s	100 ppm	30.1	24
Au@SnO ₂ core-shell structures	300 °C	3 s	—	100 ppm	76.9	2
ZnSnO ₃ nanorods	250 °C	5 s	15 s	500 ppm	109	41
Au/ZnO nanoplates	300 °C	13 s	—	5 ppm	—	42
ZnO nanoplates		135 s	—		—	
Au/ZnO nanostructures	300 °C	10 s	—	50 ppm	8.9	11 and 43
CdS NWs	206 °C	0.4 s	0.2 s	100 ppm	14.9	In this work

crystalline CdS NWs have promising applications in detecting ethanol vapor.

The gas sensing mechanism of the CdS NWs is explained as the space-charge region model, which mainly involves gas adsorption, charge transfer and desorption processes. Once the sensor is exposed to air at a high temperature, oxygen molecules can extract the electrons from the conduction band of CdS and form ionized oxygen species (O_2^- , O^- , O^{2-}), leading to a narrow conduction channel. Then, the CdS NW shows a high resistance state in air due to the formation of a space-charge region. O^- is believed to be dominant at the operating temperature around 200 °C.²³ When reductive ethanol gas molecules approach the CdS NWs surfaces, they will react with the adsorbed oxygen species and release the trapped electrons back into the NWs. Therefore, the conduction channel becomes wider, increasing the conductivity of the CdS NWs eventually:²⁴



There are several reasons for the better gas-sensing performance of the present CdS nanowire-based device: (1) compared with 0D nanoparticles and thin films, structures of 1D CdS nanowires with the larger surface-to-volume ratios and length-to-diameter ratios could be used as an important factor to explain the fast response performance.^{25,26} 1D sensing architectures provide unparalleled advantages in terms of facilitating fast mass transfer of the gas molecules to and from the interaction region. What's more, they require charge carriers to traverse any barriers introduced by molecular recognition events along the entire wire.²⁷ Therefore, the 1D architecture of CdS nanowires are considered to contribute to the extremely rapid response and recovery behavior of sensors. (2) In polycrystalline states, the carriers must overcome the many barriers created at the inter-grain contacts by thermionic emission in order to move from one grain to the other, which reduces the mobility of conduction electrons. While in a single crystalline state, the current flows parallel to the surface without overcoming many grain barriers.^{28,29} In our work, the CdS nanowire is single crystalline, there are few grain boundaries in the nanowire, which is advantageous for the quick transfer of

electrons in the sensing materials and benefits the fast response. (3) Compared with O element, the electronegativity of S element is weaker. Thus, it is easier for oxygen molecules adsorbed on the CdS surface to react with reactive chemical species S^{2-} in CdS than reactive O^{2-} in a metal oxide to form ionized oxygen species (O_2^- , O^- , O^{2-}). Therefore, the activation energy for the transformation of oxygen molecules to ionized oxygen on the CdS surface is lower than that needed on the metal oxide surface. Thus, more ionized oxygen species are formed on the CdS surface. As we know that ionized oxygen species are the bases of the gas sensing reaction, the CdS NWs sensor may need a lower working temperature than traditional metal oxide based devices.

The better sensitivity for ethanol than methanol is considered to be caused by the different optimum working temperatures of the sensor to the two gases. According to previous reports, the sensor shows selectivity at different operating temperatures due to the distinction of the orbital energy of the VOCs molecule.³⁰ The energy needed for the gas sensing reaction will reduce when the value of the LUMO energy is lower. As the value of the LUMO energy for ethanol (0.12572 eV) is reported to be lower than that of methanol (0.19728 eV), the possibility of electron transfer between the ethanol molecules and surface of CdS NWs will be larger.^{25,30} Therefore, the CdS sensor showed higher sensitivity to ethanol than methanol.

PD performance and device mechanism

As shown in Fig. 4a, a PL spectrum for the CdS NWs was taken at room temperature. The strong and sharp peak at 505 nm demonstrated in the PL spectrum is consistent with room-temperature band-edge emission from CdS,³¹ whereas the weak and broad emission band around 640 nm can be due to the luminescence of surface defects.^{10,32} The signal intensity around 640 nm is much lower than that at 505 nm, indicating that the number of defects on the NW surface is quite small. Fig. 4b shows the results of photocurrent measurements performed on CdS NWs device in the dark and under the illumination of 460 nm visible light, respectively. The I - V curve shapes are consistent with the formation of back-to-back M-S diodes due to the Schottky barrier between the Au electrodes and the CdS NWs.³³ At -4 V bias, the dark current is only 400 pA (shown in the upper left corner of Fig. 4b) while the photocurrent can

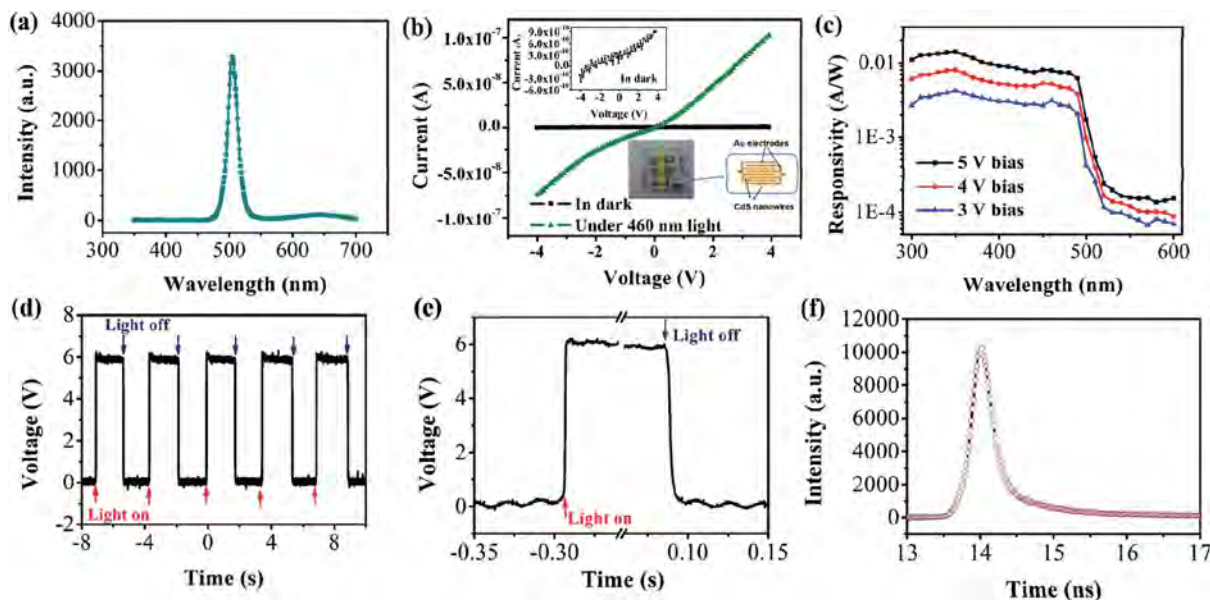


Fig. 4 (a) Room-temperature photoluminescence spectra of CdS NWs. The PL excitation wavelength was 325 nm. (b) I - V curves of the CdS-NWs PD in the dark conditions and under 460 nm light illumination, respectively. The inset in the upper left corner shows the I - V curve in the dark, while the insets in the lower right corner show the image of the CdS-NWs device (left) and the schematic diagram of the device configuration (right). (c) The photoresponse of the PD for different wavelengths. (d) Reproducible on-off switching of the device upon the pulsed incidence light created by a mechanical chopper. (e) Photovoltage vs. time plots under light irradiation (a power of 2.8 mW cm^{-2}). (f) Corresponding temporal decay of the normalized photoluminescence signal.

reach 70 nA under illumination ($\lambda = 460 \text{ nm}$, 1.57 mW cm^{-2}). The ratio of photocurrent-to-dark reaches 2 orders of magnitude, and the low room temperature dark current is strongly desirable for its practical application. The inset in the lower right corner of Fig. 4b shows an image of the CdS-NWs device (left) and the corresponding schematic diagram of a device configuration (right). In the PD, the gaps between the Au electrodes are bridged by CdS wires.

Fig. 4c displays the spectroscopic photoresponse of the sensor at different bias (3 V, 4 V, 5 V) when illuminated by different light from 300 nm to 600 nm. It can be found that the responsivity of device will get higher with the increasing of bias voltage. The low response to 520 nm light and the high response to the green light of 490 nm suggest that this device is indeed highly green light-sensitive. Similar to already reported devices, it is seen that 510 nm is the cut-off wavelength and sensitivity shows a steep decline in the long wavelength direction, indicating that the electron-hole pairs excited by light with energy larger than the band-gap of CdS should account for the photocurrent.³⁴

The rise and decay time of a PD are key parameters which determine the capability of a device to follow a fast-varying optical signal.³⁵ We recorded the response characteristics of the device using a modified test circuitry that involves a load resistance. By measuring the voltage variation in the load resistance, the results of the light variations are obtained. Fig. 4d shows the excellent stability and repeatability of the device under illumination (2.8 mW cm^{-2}). It can be found that when the light was turned on, the photovoltage rapidly increased to a stable value, then drastically decreased to its

initial level when the light turned off. By periodically turning the light on and off, the photovoltage can be reproducibly switched from the high state to the low state. No notable photovoltage degradation was observed, and the photovoltage fluctuations were very low, proving the high stability of the CdS NWs-based detector. The rise and decay time are defined as the time required for the voltage to increase from 10% to 90% of V_{max} and decrease from 90% to 10% of V_{max} , respectively. From Fig. 4e, it is known that the rise and decay times are 750 μs and 3.77 ms, respectively, which are much faster than most of the reported 1D CdS based detectors. Particularly, the decay speed is the fastest in the reported PDs based on randomly oriented CdS NW networks. A detailed comparison of the most important CdS nanostructure performances can be found in Table 2. The above-mentioned results demonstrate that the present method to fabricate ultrafast CdS NWs-based visible-light detectors is facile and effective and can be commercialized.

Several unique characteristics of the device are believed to contribute to the fast rise speed and the significantly improved decay speed as compared to previously reported CdS PDs: (1) the short lifetime of photo-generated carriers in CdS NWs is beneficial for the fast decay speed. In Fig. 4f, a sharp nonlinear decay as short as $\sim 80 \text{ ps}$ in the PL of CdS NWs is demonstrated immediately after the laser pulse, indicating that the carriers recombined quickly after being generated by light irradiation. It should be known that defects in active materials and surface states influence the recombination rate of carriers.^{35,36} In our device, the superior crystal quality of nanostructures could benefit a high decay speed because the single crystalline CdS NWs should have fewer numbers of defects than polycrystalline

Table 2 Comparison of the most important CdS nanostructure visible-light PD parameters between this work and the previous reports

Material	Method	Rise time	Decay time	Reference
Single CdS nanobelt	Thermal evaporation	91 ms	864 ms	17
Single CdS nanoribbon	Thermal evaporation	551 μ s	1.093 ms	20
Single CdS nanoribbon	Chemical vapor deposition	746 μ s	794 μ s	19
CdS nanobelts	Thermal evaporation	1 s	3 s	44
Cl-doped CdS NWS	Thermal co-evaporation	<1 s	<1 s	21
CdS NWS	PVD process	—	320 ms (white light) 57 ms (254 nm) 380 ms (365 nm)	45
CdS NWS	Vapor-liquid-solid	0.8 ms	240 ms	35
CdS NWS	Solvothermal method	750 μ s	3.77 ms	In this work

materials. What's more, the introduction of surface states induced by depositing device electrodes onto the sensing materials in traditional manufacturing processes is avoided. Thus the short lifetimes of photo-generated carriers were obtained. (2) The reduced recombination barriers in CdS nanostructures were beneficial to the rise and decay speed. It has been demonstrated that the recombination barrier height in GaN NWS decreases when the wire diameter is smaller than a critical value (100 nm for GaN NWS).¹⁹ In our CdS NWS, the diameters of which were in the range of 30–110 nm, recombination barrier height could be small. (3) The strong electrical field built by the high-quality Schottky contact between Au electrodes and CdS NWS is desired to facilitate exciton dissociation and leads to the fast response speed.³⁴

Conclusions

In summary, high-quality single-crystalline CdS NWS were prepared by a solvothermal route and were successfully used to fabricate a gas sensor for the first time. The gas sensor exhibited high sensitivity, relatively low working temperature, good selectivity, fast response (0.4 s) and recovery speeds (0.2 s) toward ethanol. The optical properties of CdS NWS were also investigated. The photo-to-dark conductance ratio of the corresponding detector was more than 10^2 under 460 nm light irradiation. The short rise and decay times of CdS NWS under light illumination are 750 μ s and 3.77 ms, respectively, which are very important for CdS NWS used in the field of optoelectronics and other fields. Our results implied that the excellent gas sensing and optical properties make the single-crystalline CdS NWS synthesized by a solvothermal method a good candidate for gas sensors and visible-light detectors with high-performance.

Acknowledgements

This work was supported by National Natural Science Foundation of China (61274068), Chinese National Programs for High Technology Research and Development (grant no. 2013AA030902), Project of Science and Technology Development Plan of Jilin Province (grant no. 20120324, 20130206021GX).

Notes and references

- L. Zhu, X. Gu, F. Qu, J. Zhang, C. Feng, J. Zhou, S. Ruan and B. Kang, *J. Am. Ceram. Soc.*, 2013, **96**, 3183–3187.
- J. Zhang, X. Liu, S. Wu, M. Xu, X. Guo and S. Wang, *J. Mater. Chem.*, 2010, **20**, 6453–6459.
- Y. Lu, W. Zhan, Y. He, Y. Wang, X. Kong, Q. Kuang, Z. Xie and L. Zheng, *ACS Appl. Mater. Interfaces*, 2014, **6**, 4186–4195.
- X. Gu, F. Meng, G. Liu, H. Zhang, J. Zhou and S. Ruan, *Chem. Commun.*, 2013, **49**, 6328–6330.
- C. Feng, W. Li, C. Li, L. Zhu, H. Zhang, Y. Zhang, S. Ruan, W. Chen and L. Yu, *Sens. Actuators, B*, 2012, **166**, 83–88.
- A. L. Pan, S. Q. Wang, R. B. Liu, C. R. Li and B. S. Zou, *Small*, 2005, **1**, 1058–1062.
- T. Zhai, X. Fang, L. Li, Y. Bando and D. Golberg, *Nanoscale*, 2010, **2**, 168–187.
- K. Deng and L. Li, *Adv. Mater.*, 2014, **26**, 2619–2635.
- L. Li, P. Wu, X. Fang, T. Zhai, L. Dai, M. Liao, Y. Koide, H. Wang, Y. Bando and D. Golberg, *Adv. Mater.*, 2010, **22**, 3161–3165.
- F. Gu, L. Zhang, H. Yu, W. Fang, J. Bao and L. Tong, *Nanotechnology*, 2011, **22**, 425201.
- F. Gu, L. Zhang, G. Wu, Y. Zhu and H. Zeng, *Nanoscale*, 2014, **6**, 12371–12375.
- A. Monkawa, T. Nakagawa, H. Sugimori, E. Kazawa, K. Sibamoto, T. Takei and M. Harutab, *Sens. Actuators, B*, 2014, **196**, 1–9.
- M. C. Steele and B. A. MacIver, *Appl. Phys. Lett.*, 1976, **28**, 687–688.
- V. Smyntyna, V. Golovanov, S. Kačiulis, G. Mattogno and G. Righini, *Sens. Actuators, B*, 1995, **25**, 628–630.
- B. T. Raut, P. R. Godse, S. G. Pawar, M. A. Chougule and V. B. Patil, *J. Mater. Sci.: Mater. Electron.*, 2012, **23**, 956–963.
- K.-T. Lin, S.-C. Tseng, H.-L. Chen, Y.-S. Lai, S.-H. Chen, Y.-C. Tseng, T.-W. Chu, M.-Y. Lin and Y.-P. Lu, *J. Mater. Chem. C*, 2013, **1**, 4244–4251.
- Q. H. Li, T. Gao and T. H. Wang, *Appl. Phys. Lett.*, 2005, **86**, 193109.
- J.-P. Kim, J. A. Christians, H. Choi, S. Krishnamurthy and P. V. Kamat, *J. Phys. Chem. Lett.*, 2014, **5**, 1103–1109.
- J. S. Jie, W. J. Zhang, Y. Jiang, X. M. Meng, Y. Q. Li and S. T. Lee, *Nano Lett.*, 2006, **6**, 1887–1892.

- 20 L. Yingkai, Z. Xiangping, H. Dedong and W. Hui, *J. Mater. Sci.*, 2006, **41**, 6492–6496.
- 21 C. Wu, J. Jie, L. Wang, Y. Yu, Q. Peng, X. Zhang, J. Cai, H. Guo, D. Wu and Y. Jiang, *Nanotechnology*, 2010, **21**, 505203.
- 22 C. Hu, X. Zeng, J. Cui, H. Chen and J. Lu, *J. Phys. Chem. C*, 2013, **117**, 20998–21005.
- 23 N. Barsan, M. Schweizer-Berberich and W. Göpel, *Fresenius' J. Anal. Chem.*, 1999, **365**, 287–304.
- 24 X. Xue, Z. Chen, C. Ma, L. Xing, Y. Chen, Y. Wang and T. Wang, *J. Phys. Chem. C*, 2010, **114**, 3968–3972.
- 25 Y. Li, J. Xu, J. Chao, D. Chen, S. Ouyang, J. Ye and G. Shen, *J. Mater. Chem.*, 2011, **21**, 12852–12857.
- 26 Q. Wan and T. H. Wang, *Chem. Commun.*, 2005, 3841–3843.
- 27 I.-D. Kim, A. Rothschild, B. H. Lee, D. Y. Kim, S. M. Jo and H. L. Tuller, *Nano Lett.*, 2006, **6**, 2009–2013.
- 28 E. Brunet, T. Maier, G. C. Mutinati, S. Steinhauer, A. Köck, C. Gspan and W. Grogger, *Sens. Actuators, B*, 2012, **165**, 110–118.
- 29 E. Comini and G. Sberveglieri, *Mater. Today*, 2010, **13**, 36–44.
- 30 Z. Wen and L. Tian-mo, *Phys. B*, 2010, **405**, 1345–1348.
- 31 X. Duan, Y. Huang, R. Agarwal and C. M. Lieber, *Nature*, 2003, **421**, 241–245.
- 32 S. Besson, T. Gacoin, C. Ricolleau, C. Jacquioid and J.-P. Boilot, *Nano Lett.*, 2002, **2**, 409–414.
- 33 J. B. D. Soole and H. Schumacher, *IEEE J. Quantum Electron.*, 1991, **27**, 737–752.
- 34 D. Wu, Y. Jiang, Y. Zhang, Y. Yu, Z. Zhu, X. Lan, F. Li, C. Wu, L. Wang and L. Luo, *J. Mater. Chem.*, 2012, **22**, 23272–23276.
- 35 K. Heo, H. Lee, Y. Park, J. Park, H.-J. Lim, D. Yoon, C. Lee, M. Kim, H. Cheong, J. Park, J. Jian and S. Hong, *J. Mater. Chem.*, 2012, **22**, 2173–2179.
- 36 D. Y. Jiang, J. Y. Zhang, K. W. Liu, Y. M. Zhao, C. X. Cong, Y. M. Lu, B. Yao, Z. Z. Zhang and D. Z. Shen, *Semicond. Sci. Technol.*, 2007, **22**, 687.
- 37 M. Cao, Y. Wang, T. Chen, M. Antonietti and M. Niederberger, *Chem. Mater.*, 2008, **20**, 5781–5786.
- 38 A. S. Kamble, R. C. Pawar, N. L. Tarwal, L. D. More and P. S. Patil, *Mater. Lett.*, 2011, **65**, 1488–1491.
- 39 L. Wang, T. Fei, Z. Lou and T. Zhang, *ACS Appl. Mater. Interfaces*, 2011, **3**, 4689–4694.
- 40 J. Huang, K. Yu, C. Gu, M. Zhai, Y. Wu, M. Yang and J. Liu, *Sens. Actuators, B*, 2010, **147**, 467–474.
- 41 H. Men, P. Gao, B. Zhou, Y. Chen, C. Zhu, G. Xiao, L. Wang and M. Zhang, *Chem. Commun.*, 2010, **46**, 7581–7583.
- 42 J. Zhang, X. Liu, S. Wu, B. Cao and S. Zheng, *Sens. Actuators, B*, 2012, **169**, 61–66.
- 43 X. Liu, J. Zhang, L. Wang, T. Yang, X. Guo, S. Wu and S. Wang, *J. Mater. Chem.*, 2011, **21**, 349–356.
- 44 T. Gao, Q. H. Li and T. H. Wang, *Appl. Phys. Lett.*, 2005, **86**, 173105.
- 45 T.-Y. Wei, C.-T. Huang, B. J. Hansen, Y.-F. Lin, L.-J. Chen, S.-Y. Lu and Z. L. Wang, *Appl. Phys. Lett.*, 2010, **96**, 013508.